

# *In silico* studies reveal potential antiviral activity of phytochemicals from medicinal plants for the treatment of COVID-19 infection

Mansi Pandit

Bioinformatics center, Sri Venkateswara College, University of Delhi

N. Latha (✉ [lata@bic-svc.ac.in](mailto:lata@bic-svc.ac.in))

Bioinformatics center, Sri Venkateswara College, University of Delhi

---

## Research Article

**Keywords:** SARS-CoV-2, Drug Targets, Phytochemicals, Medicinal Plants, Docking, Binding energy

**Posted Date:** April 14th, 2020

**DOI:** <https://doi.org/10.21203/rs.3.rs-22687/v1>

**License:**   This work is licensed under a Creative Commons Attribution 4.0 International License.

[Read Full License](#)

---

# Abstract

The spread of COVID-19 across continents has led to a global health emergency. COVID-19 disease caused by the severe acute respiratory syndrome coronavirus 2 (SARS-CoV-2) has affected nearly all the continents with around 1.52 million confirmed cases worldwide. Currently only a few regimes have been suggested to fight the infection and no specific antiviral agent or vaccine is available. Repurposing of the existing drugs or use of natural products are the fastest options available for the treatment. The present study is aimed at employing computational approaches to screen phytochemicals from the medicinal plants targeting the proteins of SARS-CoV2 for identification of antiviral therapeutics. The study focuses on three target proteins important in the life cycle of SARS-CoV-2 namely Spike (S) glycoprotein, main protease (Mpro) and RNA-dependent RNA-polymerase (RdRp). Molecular docking was performed to screen phytochemicals in medicinal plants to determine their feasibility as potential inhibitors of these target viral proteins. Of the 30 plant phytochemicals screened, Silybin, an active constituent found in *Silybum marianum* exhibited higher binding affinity with targets in SARS-CoV-2 in comparison to currently used repurposed drugs against SARS-CoV-2. Withaferin A from *Withania somnifera* also showed significant binding to the targets proteins. In addition, phytochemicals from *Tinospora cordifolia* and *Aloe barbadensis* displayed good binding energetics with the target proteins in SARS-CoV-2. These results provide a basis for the use of traditional medicinal plants as alternative lines of treatment for COVID-19 infection.

## Introduction

COVID-19 disease caused by the novel coronavirus SARS-CoV-2 has been declared as a global pandemic by WHO. Severe Acute Respiratory Syndrome Corona Virus 2 (SARS-CoV-2), previously named 2019 n-CoV, first emerged in late 2019 in China [1]. Since December 2019, COVID-19 infection has spread to nearly all the continents. According to the latest situation report released by WHO, globally 1.61 million confirmed cases and around 99690 deaths have been reported due to COVID-19 as on 11<sup>th</sup> April, 2020 [2]. India records 6634 confirmed cases and 242 deaths due to COVID-19 infection (as on 11<sup>th</sup> April, 2020) [3]. The virus has high rate of transmissibility and spreads via droplets, physical contact with infected individuals, contaminated surfaces and possibly through oral-fecal route [4]. Common symptoms of a person infected with coronavirus include fever, cough, shortness of breath, and dyspnea. In more severe cases, the infection can cause pneumonia, severe acute respiratory syndrome, kidney failure, and even death due to multiple organ failure [5].

SARS-CoV-2 is an enveloped RNA virus belonging to the *Coronaviridae* family and genus beta-coronavirus and is distant from SARS-CoV with 79% identity. Phylogenetic analysis of the SARS-CoV-2 shows 50% identity with Middle East respiratory syndrome coronavirus MERS-CoV, 88% identity to two bat-derived (SARS)-like coronaviruses bat-SL-CoVZC45 and bat-SL-CoVZXC21 [6] and 96.2% identity to bat CoV RaTG13 [7]. The complete genome of Wuhan-Hu-1 coronavirus (WHCV), a strain of SARS-CoV2

with a size of 29.9 kb was first isolated from a pneumonia patient in Wuhan [8]. The genome has variable number of Open reading frames (around 6–11) [9]. Viral RNA located in the ORF1 translates two polyproteins, pp1a and pp1ab, and encodes 16 non-structural proteins (NSP), while remaining ORF codes for structural proteins. Corona virus has four major structural proteins, namely the Spike (S) protein, envelope (E) protein, membrane (M) protein, and nucleocapsid (N) protein [10]. Among these, S glycoprotein of SARS-CoV-2 binds to host cell receptors, angiotensin-converting enzyme 2 (ACE2) that is a critical step for virus entry [11]. Both the structural proteins and NSPs have played important roles from drug design perspectives. The therapies for SARS-CoV-2 can target different pathways—structural proteins that block the entry of virus into the human host cell, critical enzymes involved in viral replication and virus RNA synthesis, proteins that cause virulence or aid virus assembly process and many more. Availability of crystal structures of SARS-CoV-2 proteins in PDB (*Table 1*) has guided structure-based drug design endeavors for development of antiviral agents.

To date, no specific therapeutic drug or vaccine has been approved for the treatment of coronavirus. There is an urgent need to discover novel antivirals for the ongoing pandemic situation caused by Severe Respiratory Corona Virus 2 (SARS-Cov-2). Drug discovery for the very infectious COVID-19 is a challenging job owing to frequent mutations [12]. In addition, researchers across the globe are racing to develop potential vaccines [13]. The development of both novel antiviral compounds as well as vaccines presents several challenges and requires significant amounts of effort and time for validation. Therefore, exploring the repurposing of already-approved pharmaceuticals or the use of natural compounds can provide alternatives to the development of novel antiviral drugs. Chloroquine, a repurposed drug known widely for the treatment of malaria is used to treat COVID-19 infection [14]. *In vitro* studies have shown

hydroxychloroquine, a less hepatotoxic derivative of chloroquine, to be foremost effective drug in inhibiting SARS-CoV-2 infection [15]. Few clinical trials have also shown chloroquine phosphate to be effective in COVID-19 associated pneumonia [16]. Other antivirals in combination or alone are also being used to determine their effectiveness against SARS-CoV-2 [17–18]. However, at present the treatment is only symptomatic and more effective antivirals need to be developed to fight the deadly disease.

Medicinal plants are valuable sources of drugs used globally as alternative medicines. India is a rich source of biodiversity with more than 7000 plants species used as medicinal plants [19].

India also has a rich ancient tradition of alternative medicines – Ayurveda, Yoga, Unani and Siddha and Homeopathy system (AYUSH) that is still in use today. It has also been estimated that 70- 80 % of people in developing countries are totally dependent on herbal drugs for their primary healthcare [20]. Traditional medicinal plants with strong antiviral activity have long been used to treat viral infection [21–22]. The beneficial medicinal effects of plant products typically result from the secondary metabolites present in the plants. A variety of phytochemicals derived from the plant like alkaloids, steroids, diterpenoid lactones, aliphatics, and glycosides have proved to induce antiviral effects in humans [23]. The world has started exploring traditional medicines for the treatment of viral diseases, which are comparatively more economical, easily available and bear fewer chances of side effects and toxicity [24].

Bioinformatics and systems biology approaches can aid to study the therapeutic potential of traditional medicinal plants, making drug development faster, cheaper, and safer [25]. Receptors and enzymes involved in various stages in the life cycle of the SARS-CoV-2 are being used as drug targets. Viral proteases have long been shown to be effective targets of antiviral therapies as seen in case of human immunodeficiency virus (HIV) and hepatitis C virus (HCV) infections. Proteases represent potential targets for the inhibition of viral replication, One of the best characterized drug targets among coronaviruses is the main protease (M<sup>Pro</sup>, also called 3CL<sup>Pro</sup>) [26]. The protein sequences of the SARS-CoV-2 M<sup>Pro</sup> and the SARS-CoV M<sup>Pro</sup> show 96% identity [27]. The functional importance of M<sup>Pro</sup> in the viral life cycle, together with the absence of closely related homologues in humans, identifies M<sup>Pro</sup> as an attractive target for antiviral drug design. Many of the protease inhibitors are being used in the treatment of COVID-19, e.g., lopinavir-ritonavir combinations [28-29]. Recent studies have also reported the importance of viral Spike (S) protein in receptor binding and shown that human angiotensin-converting enzyme 2 (ACE2) promotes entry of SARS-CoV-2 into the cells [30]. Spike proteins offer as excellent drug targets at the early infection stage. Angiotensin-converting enzyme 2 (ACE2) binds to the receptor-binding motif (RBM) in the receptor-binding domain (RBD) of S protein and functions as a receptor for SARS-CoV [31-32]. Many inhibitors have been proposed that block the binding of spike proteins protein to ACE2 receptor in the human host. Repurposing of drug Nafamostat mesylate (Fusan), used to treat acute pancreatitis, has showed inhibition of MERS-SARS entry in human cells [33]. Targeting RNA-dependent RNA-polymerase (RdRp), required for viral RNA replication is another good choice for the development of antiviral therapeutics. It has been targeted in the development of therapeutics for several viral infections, including the hepatitis C virus (HCV), the Zika virus (ZIKV), and coronaviruses (CoVs) [34-42].

India is a country rich with diverse repository of medicinal plants used for treatment of several human disorders. *Tinospora cordifolia* also known as *amrita*, *guduchi*, *shindilkodi*, *giloy*, is widely used in indigenous systems of Indian medicine [43]. The chemical constituents of *T. cordifolia* belong to different classes, namely terpenoids, alkanoids, glycosides, lignans, steroids among others [43-45]. The natural phytochemicals found in *Tinospora cordifolia* are known to show antiviral activity for many viral infections [46-48]. Curcumin, a component of turmeric (*Curcuma longa*) has been described to have several functions in preventing or treating diseases, including cancers and viral infections [49]. It has also been demonstrated that curcumin is an antiviral compound, with activity against diverse viruses such as dengue virus (serotype 2) [50], herpes simplex virus [51], human immunodeficiency virus [52], Zika and Chikungunya [53] among others. Curcumin and its analogues have proved to be useful as HIV-1 integrase inhibitor [51, 54]. *Aloe Barbadensis* (Aloe Vera) has been used medicinally for several thousands of years in many cultures; from ancient Egypt, Greece, and Rome to China and India. For centuries, the gel of Aloe vera has been used for healing and therapeutic purposes [55]. The biologically active components include anthraquinones, anthrones, chromanes, alkaloids, flavonoids, terpenes, minerals, carbohydrates and pyrans. An extract of Aloe Vera has been found to be effective against a broad range of viruses, especially causing the infections of the upper respiratory tract [56]. Anthraquinones isolated from Aloe vera has shown to inhibit herpes simplex virus-2 [57], hepatitis virus [58], Influenza virus [59] and Human Immunodeficiency virus HIV [60]. It has also been reported that consumption of A. vera might be helpful

to human immunovirus-infected individuals since it enhances the CD4 count and thereby improves the functioning of the immune system. [60]. Lignans are a class of natural products that possess diverse pharmacological properties and are known to be effective as antitumor, antioxidant, antibacterial and antiviral agents [61]. Milk thistle (*Silybum marianum*) is another medicinal plant that has been used for thousands of years as a remedy for a variety of ailments [62]. The major component of *S. marianum* fruit extract (silymarin) is a flavonoid lignan called silybin that has been used in Indian medicines for liver and gallbladder problems [63–64]. Many studies have also reported that silymarin is an effective antiviral treatment for hepatitis C virus (HCV) [65–66]. *Withania somnifera* (Ashwagandha) is one of the most important herbs of Ayurvedic system of Indian medicine [67]. Withaferin A (WA) is an active constituent of *Withania somnifera* that has been shown to have a broad range of medicinal properties including antiviral activity [68–69]. Withanolides are steroidal lactones present in ashwagandha possessing diverse pharmacological activities [70].

Based on the above observations, this work focused on the study of phytochemicals derived from the medicinal plants for their antiviral activity towards SARS-CoV-2. The targets were carefully identified that played a key role in the viral attachment to host cell, viral replication and viral synthesis. A library of 30 natural metabolites in medicinal plants included curcumin and its derivatives, chemical constituents of giloy (*Tinospora cordifolia*), *Aloe Barbadensis*, *S. marianum*, *Withania somnifera* and plant lignans were studied by docking to three targets Main protease, Spike S protein and RNA dependent RNA polymerase (RdRp) in SARS-CoV-2. In addition to the library of phytochemicals, we also included the currently used hydroxychloroquine along with other repurposed drugs as ligands for molecular docking.

## Methodology

### *Retrieval of Structures of Target Proteins*

The three-dimensional structures of protein targets from SARS-Cov-2 were retrieved from Protein Data Bank [71]. Targets chosen for this study included SARS-CoV-2 main protease (PDB ID: 6W63) [72], Spike receptor binding domain (PDB ID: 6M0J) [73] and RNA-dependent RNA-polymerase (RdRp) (PDB ID: 6M71) [74] crucial for the viral entry and replication.

### *Ligand Preparation*

A library of phytochemicals in medicinal plants was compiled as ligands from the review of literature and their 2D structures were retrieved from PubChem database [75]. For the ligands whose structures were not available, the 2D structures were drawn using MarvinSketch [76]. The protein and ligand structures were prepared using the preparation wizard in Flare (module from CRESSET software) [77–78].

### *Prediction of Binding site*

Binding site of the main protease was analyzed by using the information about the amino acid residues interacting with the known, co-crystallized ligand. The interface residues of the spike receptor binding

domain with ACE2 (Angiotensin converting enzyme 2) were selected for grid generation for spike protein. The binding site for RNA-dependent RNA-polymerase (RdRp) was predicted using CASTp web server [79].

### *Protein-Ligand Molecular Docking*

Molecular docking of the ligand library composed of natural compounds and repurposed drugs currently in use for COVID-19 treatment was carried out with target proteins main protease, spike protein (S) and RNA-dependent RNA-polymerase (RdRp) using Flare module provided by CRESSET software. For the docking process, the targets were prepared and minimized, the grid box was defined according to the binding site information and the docking calculations were carried out in Cresset Flare software in normal mode and default settings.

## Results And Discussion

Molecular docking of target proteins namely main protease, spike protein and RNA-dependent RNA-polymerase from SARS-CoV-2 was performed with ligands using Flare docking protocol that use the polarizable extended electron distribution (XED) force field [78]. A library of ligands comprising of 30 phytochemicals from medicinal plants *Tinospora cordifolia*, *Aloe Barbadensis*, *Withania somnifera*, *Silybum marianum* and plant lignans along with seven repurposed drugs including hydroxychloroquine currently in use for COVID-19 treatment (Table 3) were prepared for docking. The amino acid residues of target proteins considered for binding during molecular docking are enlisted in Table 4. It was observed that several phytochemicals screened showed significant binding to the target proteins of SARS-CoV-2 upon docking in comparison to hydroxychloroquine and other antiviral drugs binding. Analysis of molecular docking revealed Silybin (flavonolignan), the major active component of silymarin (from *Silybum marianum*) to be the most promising inhibitor of the target proteins in SARS-CoV-2. Significant binding energy values of -11.928 kcal/mol with Silybin-main protease complex, -10.572 kcal/mol with Silybin-S spike glycoprotein complex and -11.499 kcal/mol with Silybin-RNA-dependent RNA-polymerase were estimated (Figure 1). To obtain deeper insight into interaction pattern of silybin with target proteins, protein-ligand interaction maps were plotted and key amino acid residues involved in interactions were identified. The interaction plot of main protease complexed with silybin highlighted Thr 25, Met 49, His 163 and Glu 166 as important residues involved in hydrogen bonding (Figure 2a). In the spike protein/ACE2-silybin docked complex, strong hydrogen bonds were formed by residues Lys 353, Arg 403, Tyr 453, Ser 494 and amino acid residue like His 34 was observed to be involved in aromatic-aromatic interaction with the ligand (Figure 2b). Stable hydrogen bonds were also seen in RdRp-silybin dock complex formed by residues Val 315, Thr 394, Arg 457, Asn 459 and Asn 628 (Figure 2c).

Withaferin A, a major pharmacological constituent from Ashwagandha (*Withania somnifera*) also displayed very strong binding with main protease having binding energy value of -11.242 kcal/mol. Analysis of interaction interface in the active site showed hydrogen bond formation of the compound with residues Cys 44 and Glu 166 in the main protease. Amino acid residues Glu 35 and Gln 42 in spike protein/ACE2 participated in hydrogen bond formation with Withaferin A which contributed to a binding

energy value of  $-9.631$  kcal/mol. On the other hand, in RdRp-Withaferin A docked complex, amino acid residues Lys 621, Asp 623, Glu 811 and Ser 814 mediated hydrogen bond interactions with a total binding energy value of  $-9.27$  kcal/mol. Glu 166 in the main protease was identified as a key residue facilitating strong interactions with ligands analyzed by docking. Withanolide A found in *Withania somnifera* showed significant interaction with main protease ( $-10.292$  kcal/mol) and RdRp ( $-9.668$  kcal/mol). The results also implicated that compounds like catechin (phenolic constituent from aloe vera plant) and phillygenin (lignan) showed significant interaction with protease (Table 5). In addition, cordioside, a phytochemical constituent in *Tinospora cordifolia*, interacted strongly with the main protease having binding energy value of  $-10.577$  kcal/mol. Furthermore, quercetin, a constituent of Aloe vera, displayed good binding with RNA-dependent RNA-polymerase with an energy value of  $-9.131$  kcal/mol. The above results implicate the antiviral activity of medicinal plants that can aid in treatment of COVID-19 infection

## Conclusion

Highly pathogenic viruses such as SARS-Corona pose a significant threat to human health, yet in most cases, therapies to prevent or treat these diseases are lacking. The COVID-19 outbreak is an unprecedented global public health challenge and needs immediate intervention. With the current threat looming over the world, there is urgency to develop both effective diagnostics and newer therapeutics at an affordable cost with minimum or no side effects. Structural bioinformatics has emerged during the last thirty years as a powerful tool for rational drug discovery. In this context, three-dimensional structures of target proteins have played essential roles for the design and discovery of newer or alternative drugs. Traditional Indian medicinal plants have long been used for treatment of several diseases including antiviral therapeutics against several viruses. This study observed that phytochemicals in medicinal plants displayed better binding affinities than the synthetic repurposed drugs currently in use for treatment for COVID-19 infection. Among the phytochemicals screened, natural compounds derived from *Silybum marianum* (Silybin), *Withania somnifera* (Withaferin A), *Tinospora cordifolia* (Cordioside) and *Aloe Barbadensis* Catechin and Quercetin) exhibited higher binding energetics than the widely used hydroxychloroquine and other repurposed drugs used for treatment of COVID-19 infection. The proposed *in silico* studies hence suggest the medicinal plants extracts or as an herbal cocktail could serve as effective alternative therapeutics for treatment of COVID-19 affected patients. However this would require validation from clinical cases tested upon. In addition, many more such bioactive components from medicinal plants existing in the rich Indian biodiversity need to be further explored. This study could provide basis for alternative therapeutics against the invading biological pathogens including the currently threatening coronavirus SARS-CoV-2.

## Declarations

### Acknowledgements

Authors acknowledge Department of Biotechnology (DBT-BTISNET), Government of India for financial support.

## Conflict of interest

Authors declare no conflict of Interest

## References

1. Zhu N, Zhang D, Wang W, Li X, Yang B, Song J, et al. (2019). China Novel Coronavirus Investigating and Research Team. A Novel Coronavirus from Patients with Pneumonia in China, *N Engl J Med*, 382(8):727–33.
2. <https://www.who.int/emergencies/diseases/novel-coronavirus-2019>
3. <https://coronavirus.jhu.edu/map.html>
4. Bai Y, Yao L, Wei T, Tian F, Jin DY, Chen L, et al. (2020). Presumed asymptomatic carrier transmission of COVID-19. *JAMA*. [Epub ahead of print].
5. Wang D, Hu B, Hu C, Zhu F, Liu X, Zhang J, et al. Clinical characteristics of 138 hospitalized patients with 2019 novel coronavirus-infected pneumonia in Wuhan, China. (2020). *JAMA*, 323(11):1061.
6. Lu R, Zhao X, Li J, Niu P, Yang B, Wu H, et al. (2020). Genomic characterisation and epidemiology of 2019 novel coronavirus: implications for virus origins and receptor binding. *Lancet*, 395(10224):565–74
7. Guo Y, Cao Q, Hong Z. et al. (2020). The origin, transmission and clinical therapies on coronavirus disease 2019 (COVID-19) outbreak – an update on the status. *Military Med Res*, 7(11). <https://doi.org/10.1186/s40779-020-00240-0>
8. Wu F, Zhao S, Yu B, Chen YM, Wang W, Song ZG, et al. (2020). A new coronavirus associated with human respiratory disease in China. *Nature*.
9. Song Z, Xu Y, Bao L, Zhang L, Yu P, Qu Y, et al. (2019). From SARS to MERS, thrusting coronaviruses into the spotlight. *Viruses*, 11(1):E59. <https://doi.org/10.3390/v11010059>.
10. Cui J, Li F, Shi ZL. (2019). Origin and evolution of pathogenic coronaviruses. *Nat Rev Microbiol*, 17(3):181–92.
11. Wu A, Peng Y, Huang B, Ding X, Wang X, Niu P, et al. (2020). Genome composition and divergence of the novel coronavirus (2019-nCoV) originating in China. *Cell Host Microbe*.
12. Zhang L, Shen FM, Chen F, Lin Z. (2020). Origin and evolution of the 2019 novel coronavirus. *Clin Infect Dis*.
13. Amanat F, Krammer F. (2020). SARS-CoV-2 Vaccines: Status Report. *Immunity*.
14. Vincent MJ, Bergeron E, Benjannet S, Erickson BR, Rollin PE, Ksiazek TG, et al. (2005). Chloroquine is a potent inhibitor of SARS coronavirus infection and spread. *Virol J*, 2:69.
15. Liu J, Cao R, Xu M. et al. (2020). Hydroxychloroquine, a less toxic derivative of chloroquine, is effective in inhibiting SARS-CoV-2 infection in vitro. *Cell Discov* 6, <https://doi.org/10.1038/s41421-020-0156-0>.



16. Gao J, Tian Z, Yang X. (2020). Breakthrough: Chloroquine phosphate has shown apparent efficacy in treatment of COVID-19 associated pneumonia in clinical studies, *BioScience Trends*, Article ID 2020.01047, [Advance publication].
17. Agostini ML, Andres EL, Sims AC, Graham RL, Sheahan TP, Lu X, et al. (2018). Coronavirus susceptibility to the antiviral remdesivir (gs-5734) is mediated by the viral polymerase and the proofreading exoribonuclease. *MBio*, 9(2):e00221–18.
18. Chu CM, Cheng VC, Hung IF, Wong MM, Chan KH, Chan KS, et al. (2004). Role of lopinavir/ritonavir in the treatment of SARS: initial virological and clinical findings. *Thorax*, 59(3):252–6.
19. <https://www.nmpb.nic.in/content/medicinal-plants-fact-sheet>
20. Hamilton AC. Medicinal plants, conservation and livelihoods. (2004). *Biodivers Conserv*, 13:1477–517.
21. Hudson, J.B. (1990). *Antiviral Compounds from Plants*. Boca Raton, Ann Arbor, Boston: CRC Press
22. Pankaj G. (2013). Antiviral Potential of Medicinal Plants. An overview. *International Research Journal of Pharmacy*. 4. 8-16. 10.7897/2230-8407.04603
23. Chikezie PC, Ibegbulem CO and Mbagwu FN (2015). Bioactive Principles from Medicinal Plants. *Research Journal of Phytochemistry*, 9: 88-115.
24. Barlow DJ, Buriani A, Ehrman T, Bosisio E, Eberini I and Hylands PJ. (2012). In-silico studies in Chinese herbal medicines' research: evaluation of in-silico methodologies and phytochemical data sources, and a review of research to date. *Ethnopharmacol*, 2012, **140**, 526.
25. Jin Z, Du X, Xu Y, et al. Structure of Mpro 1 from COVID-19 virus and discovery of its inhibitors. <https://doi.org/10.1101/2020.02.26.964882>.
26. K Anand, J Ziebuhr, P Wadhvani, JR Mesters, R Hilgenfeld. (2003). Coronavirus main proteinase (3CL<sup>Pro</sup>) structure: Basis for design of anti-SARS drugs. *Science* 300, 1763–1767. doi:10.1126/science.1085658 pmid:12746549.
27. Liu and XJ Wang. (2020). “Potential inhibitors against 2019-nCoV coronavirus M protease from clinically approved medicines,” *J. Genet. Genomics*, doi: 10.1016/j.jgg.2020.02.001.
28. Lim J, Jeon S, Shin HY, Kim MJ, Seong YM, Lee WJ, et al.(2020). Case of the index patient who caused tertiary transmission of COVID-19 infection in Korea: The application of lopinavir/ritonavir for the treatment of COVID-19 infected pneumonia monitored by quantitative RT-PCR. *J Korean Med Sci*, 35:e79.
29. Lan J, Ge J, Yu J. *et al.* (2020). Structure of the SARS-CoV-2 spike receptor-binding domain bound to the ACE2 receptor. *Nature*. <https://doi.org/10.1038/s41586-020-2180-5>.
30. Li W, Moore MJ, Vasilieva N, Sui J, Wong SK, Berne MA, Somasundaran M, Sullivan JL, Luzuriaga K, Greenough TC, Choe H, Farzan M. (2003). Angiotensin-converting enzyme 2 is a functional receptor for the SARS coronavirus. *Nature*, 426:450–454.
31. Tai W, He L, Zhang X. et al.(2020). Characterization of the receptor-binding domain (RBD) of 2019 novel coronavirus: implication for development of RBD protein as a viral attachment inhibitor and

- vaccine. Cell Mol Immunol, <https://doi.org/10.1038/s41423-020-0400-4>.
32. Yamamoto M, Matsuyama S, Li X, Takeda M, Kawaguchi Y, Inoue J, Matsuda Z. (2016). Identification of Nafamostat as a Potent Inhibitor of Middle East Respiratory Syndrome Coronavirus S Protein-Mediated Membrane Fusion Using the Split-Protein-Based Cell-Cell Fusion Assay Antimicrobial Agents and Chemotherapy, 60 (11) 6532-6539; DOI:1128/AAC.01043-16.
  33. Elfiky AA. (2016). Zika viral polymerase inhibition using anti-HCV drugs both in market and under clinical trials. J Med Virol, 88:2044–2051.
  34. Elfiky AA. (2017). Zika virus: novel guanosine derivatives revealed strong binding and possible inhibition of the polymerase. Futur Viro, 12:721–728.
  35. Elfiky AA. (2019). Novel guanosine derivatives as anti-HCV NS5b polymerase: a QSAR and molecular docking study. Med Chem,15:130–137.
  36. Elfiky AA, Elshemey WM (2016). IDX-184 is a superior HCV direct-acting antiviral drug: a QSAR study. Med Chem Res, 25:1005–1008.
  37. Elfiky AA, Elshemey WM. (2018). Molecular dynamics simulation revealed binding of nucleotide inhibitors to ZIKV polymerase over 444 nanoseconds. J Med Virol, 90:13–18.
  38. Elfiky AA, Elshemey WM, Gawad WA, Desoky OS. (2013). Molecular modeling comparison of the performance of NS5b polymerase inhibitor (PSI-7977) on prevalent HCV genotypes. Protein J, 32:75–80.
  39. Elfiky AA, Ismail A. (2019). Molecular dynamics and docking reveal the potency of novel GTP derivatives against RNA dependent RNA polymerase of genotype 4a HCV. Life Sci, 238.
  40. Elfiky AA, Ismail AM. (2017). Molecular modeling and docking revealed superiority of IDX-184 as HCV polymerase inhibitor. Futur Viro,12:339–347.
  41. Ganesan A, Barakat K. (2017). Applications of computer-aided approaches in the development of hepatitis C antiviral agents. Expert Opin Drug Discovery, 12:407–425.
  42. Sivarajan VV and Balachandean I. (1999). Ayurvedic Drugs and Their Plants Sources, Oxford and IBH Publishing, New Delhi, India.
  43. Panchabhai T, Kulkarni U and R Nirmala R. (2008). Validation of therapeutic claims of *Tinospora cordifolia*: A review. Phytotherapy research : PTR. 22. 425-41. 10.1002/ptr.2347.
  44. Singh SS, Pandey SC, Srivastava S, Gupta VS, Patro B, and Ghosh AC. (2003). Chemistry and medicinal properties of *Tinospora cordifolia* (Guduchi). Indian Journal of Pharmacology, vol. 35, no. 2, pp. 83–91.
  45. Ramaiah M, Kandula V, Vallepuri B, Navuluri H and Kollu H. (2018). Preliminary Phytochemical Analysis and In vitro Antiviral Activity of Ethanolic extract of Whole plant of *Tinospora cordifolia* (Thunb.) Miers against Hepatitis-A Virus. International Journal of Scientific Research in Biological Sciences. 5. 51-55. 10.26438/ijrsrbs/v5i3.5155.
  46. Kalikar MV, Thawani VR, Varadpande UK, Sontakke SD, Singh RP, Khiyani RK. (2008). Immunomodulatory effect of *Tinospora cordifolia* extract in human immuno-deficiency virus positive

- patients. Indian J Pharmacol, 40:107–10.
47. Akhtar S. (2010). Use of *Tinospora cordifolia* in HIV infection. Indian J Pharmacol. 2010; 42:57.
48. S Shome, AD Talukdar, MD Choudhury, MK Bhattacharya, H Upadhyaya. (2016). **Curcumin as potential therapeutic natural product: a nanobiotechnological perspective.** J Pharm Pharmacol, 10.1111/jphp.12611n/a-n/a.
49. Padilla SL, Rodríguez A, Gonzales MM, Gallego GJC, Castaño OJC. (2013). **Inhibitory effects of curcumin on dengue virus type 2-infected cells *in vitro*.** Arch Virol, 159, pp. 573-579, 10.1007/s00705-013-1849-6.
50. Kutluay SB, Doroghazi J, Roemer ME, Triezenberg SJ. (2008). **Curcumin inhibits herpes simplex virus immediate-early gene expression by a mechanism independent of p300/CBP histone acetyltransferase activity.** Virology, 373, pp. 239-247, 10.1016/j.virol.2007.11.028.
51. Mazumder A, Raghavan K, Weinstein J, Kohn KW, Pommier Y. (1995). Inhibition of human immunodeficiency virus type-1 integrase by curcumin. Biochem Pharmacol, 49, pp. 1165-1170.
52. Mounce BC et al. (2017). Curcumin inhibits Zika and chikungunya virus infection by inhibiting cell binding. *Antiviral Research*, Volume 142, Pages 148-157.
53. Mazumder A, Wang S, Neamati N, Nicklaus M, Sunder S, Chen J, Milne GW, Rice WG, TR Burke and Pommier Y. (1996). J Med Chem, 39, 2472–2481.
54. Maan AA, Nazir A, Khan MKI, Ahmad T, Zia R, Murid M and Abrar A. (2018). The therapeutic properties and applications of Aloe vera: A review. Journal of Herbal Medicine, 12, 1–10. <https://doi.org/10.1016/j.hermed.2018.01.002>.
55. Saalmüller G, Fal B, Schönknecht AM, Conrad K, Sievers FH and Saalmüller A. (2015). Antiviral activity of an aqueous extract derived from *Aloe arborescens* against a broad panel of viruses causing infections of the upper respiratory tract. Phytomedicine, 22, 911–920.
56. Zandi K, Zadeh MA, Sartavi K and Rastian Z. (2007). Antiviral activity of *Aloe vera* against herpes simplex virus type 2: An in vitro study. African Journal of Biotechnology, 6, 1770–1773.
57. Parvez MK, Al-Dosari MS, Alam P, Rehman M, Alajmi MF, Alqahtani AS. (2019). The anti-hepatitis B virus therapeutic potential of anthraquinones derived from Aloe vera. Phytother Res. 2019 Nov; 33(11):2960-2970. doi: 10.1002/ptr.6471.
58. Li SW, Yang TC and Lai CC. (2014). Antiviral activity of aloe-emodin against influenza A virus via galectin-3 up-regulation. European Journal of Pharmacology, 27, 125–132.
59. Olatunya OS, Olatunya AM, Anyabolu HC, Adejuyigbe EA and Oyelami OA. (2012). Preliminary Clinical Trial Indicates Aloe May Be Beneficial for Patients with HIV. The Journal of Alternative and Complementary Medicine. 850-853. <http://doi.org/10.1089/acm.2010.0735>
60. Cui Q, Du R, Liu M and Rong L (2020). Lignans and Their Derivatives from Plants as Antivirals. Molecules, 25, 183; doi: 10.3390/molecules25010183.
61. Rainone F. (2005). Milk thistle. Am Fam Physician, 72:1285–1288.

62. Abenavoli L, Capasso R, Milic N, Capasso F. (2010). Milk thistle in liver diseases: Past, present, future. *Phytother Res*, 24:1423–1432. doi: 10.1002/ptr.3207.
63. Bijak M. (2017). Silybin, a Major Bioactive Component of Milk Thistle (*Silybum marianum* Gaernt.)—Chemistry, Bioavailability, and Metabolism. *Molecules*, 22(11): 1942. doi: 10.3390/molecules22111942.
64. Biermer M, Schlosser B, Fülöp B, van Bömmel F, Brodzinski A, Heyne R, Keller K, Sarrazin C, Berg T. (2012). High-dose silibinin rescue treatment for HCV-infected patients showing suboptimal virologic response to standard combination therapy. *J. Viral Hepat*, 19, 547–553.
65. Payer B, Reiberger T, Rutter K, Beinhardt S, Staettermayer A, Peck-Radosavljevic M, Ferenci P. (2010), Successful HCV eradication and inhibition of HIV replication by intravenous silibinin in an HIV-HCV coinfecting patient. *J Clin Virol*, 49, 131–133.
66. Neumann U, Biermer M, Eurich D, Neuhaus P, Berg T. (2010). Successful prevention of hepatitis C virus (HCV) liver graft reinfection by silibinin mono-therapy. *J Hepatol*, 52, 951–952.
67. Mishra LC, Singh BB and Dagenais S. (2000). Scientific basis for the therapeutic use of *Withania somnifera* (ashwagandha): a review. *Alternative medicine review: a journal of clinical therapeutic*, 5 4, 334-46 .
68. Cai Z, Zhang G, Tang B. et al.(2015). Promising Anti-influenza Properties of Active Constituent of *Withania somnifera* Ayurvedic Herb in Targeting Neuraminidase of H1N1 Influenza: Computational Study. *Cell Biochem Biophys* 72, 727–739.
69. Kambizi, L., Goosen, B.M., Taylor, M.B., & Afolayan, A.J.. (2007). Anti-viral effects of aqueous extracts of *Aloe ferox* and *Withania somnifera* on herpes simplex virus type 1 in cell culture. *South African Journal of Science*, 103(9-10), 359-360.
70. Verma SK and Kumar A. (2011). Therapeutics uses of *Withania somnifera* (ashwagandha) with a note on withanolides and its pharmacological actions. *Asian journal of pharmaceutical sciences*, 4, suppl 1, 1-4.
71. Bernstein FC, Koetzle TF, Williams GJB et al. (1977). The protein data bank: a computer based archival file for macromolecular structures. *European Journal of Biochemistry*, vol. 80, no. 2, pp. 319–324.
72. Mesecar AD. (2020). A taxonomically-driven approach to development of potent, broad-spectrum inhibitors of coronavirus main protease including SARS-CoV-2 (COVID-19).
73. Lan J, Ge J, Yu J, Shan S, Zhou H, Fan S, Zhang Q, Shi X, Wang Q, Zhang L, Wang X. (2020). Structure of the SARS-CoV-2 spike receptor-binding domain bound to the ACE2 receptor.
74. Gao Y, Yan L, Huang Y, Liu F, Cao L, Wang T, Wang Q, Lou, Z, Rao Z. (2020). Structure of 2019-nCoV RNA-dependent RNA polymerase in complex with cofactors at 2.9 Angstroms resolution.
75. Kim S, Chen J, Cheng T, Gindulyte A, He J, He S, Li Q, Shoemaker BA, Thiessen PA, Yu B, Zaslavsky L, Zhang J, Bolton EE. PubChem 2019 update: improved access to chemical data. *Nucleic Acids Res*. 2019 Jan 8; 47(D1):D1102-1109. doi:10.1093/nar/gky1033.
76. MarvinSketch, ChemAxon (<http://www.chemaxon.com>)

77. Flare, Cresset Litlington, Cambridgeshire, UK; <http://www.cresset-group.com/flare/>; Cheeseright T, Mackey M, Rose S, Vinter, A. (2006). Molecular Field Extrema as Descriptors of Biological Activity: Definition and Validation. *J Chem Inf Model*, 46 (2), 665-676.
78. Bauer MR, Mackey MD. (2019). Electrostatic Complementarity as a Fast and Effective Tool to Optimize Binding and Selectivity of Protein–Ligand Complexes. *J Med Chem*, 62, 6, 3036-3050.
79. Tian W, Chen C, Lei X, Zhao J, Liang J. (2018). CASTp 3.0: computed atlas of surface topography of proteins. *Nucleic Acids Res*, 46(W1):W363-W367. doi: 10.1093/nar/gky473.

## Tables

**Table 1: List of crystal structures of SARS-CoV-2 proteins in PDB.**

PDB ID	Description
6VWW	Crystal Structure of NSP15 Endoribonuclease from SARS CoV-2.
6VXS	Crystal Structure of ADP ribose phosphatase of NSP3 from SARS CoV-2
6VXX	Structure of the SARS-CoV-2 spike glycoprotein (closed state)
6VYB	SARS-CoV-2 spike ectodomain structure (open state)
6W4B	The crystal structure of Nsp9 RNA binding protein of SARS CoV-2
6W9C	The crystal structure of papain-like protease of SARS CoV-2
5R8T	PanDDA analysis group deposition of ground-state model of SARS-CoV-2 main protease screened against DSI poised (Enamine), Fraglites and Peplites (Newcastle university), Mini Frags (Astex), York 3D (York university), electrophile cysteine covalent (Weizman institute) fragment libraries
6W41	Crystal structure of SARS-CoV-2 receptor binding domain in complex with human antibody CR3022
5RE4	Crystal Structure of SARS-CoV-2 main protease in complex with Z1129283193
5RFJ	Crystal Structure of SARS-CoV-2 main protease in complex with PCM-0103067
5RFI	Crystal Structure of SARS-CoV-2 main protease in complex with PCM-0102353
5RFH	Crystal Structure of SARS-CoV-2 main protease in complex with PCM-0102277
5RFG	Crystal Structure of SARS-CoV-2 main protease in complex with PCM-0102372
5RFF	Crystal Structure of SARS-CoV-2 main protease in complex with PCM-0102704
5RFE	Crystal Structure of SARS-CoV-2 main protease in complex with Z509756472
5RFD	Crystal Structure of SARS-CoV-2 main protease in complex with Z126932614
5RFC	Crystal Structure of SARS-CoV-2 main protease in complex with Z979145504
5RFB	Crystal Structure of SARS-CoV-2 main protease in complex with Z1271660837
5RFA	Crystal Structure of SARS-CoV-2 main protease in complex with Z2643472210
5RF9	Crystal Structure of SARS-CoV-2 main protease in complex with Z217038356
5RF8	Crystal Structure of SARS-CoV-2 main protease in complex with Z271004858
5RF7	Crystal Structure of SARS-CoV-2 main protease in complex with Z316425948_minor
5RF6	Crystal Structure of SARS-CoV-2 main protease in complex with Z1348371854
5RF5	Crystal Structure of SARS-CoV-2 main protease in complex with Z3241250482
5RF4	Crystal Structure of SARS-CoV-2 main protease in complex with Z1741982125
5RF3	Crystal Structure of SARS-CoV-2 main protease in complex with Z1741970824
5RF2	Crystal Structure of SARS-CoV-2 main protease in complex with Z1741969146
5RF1	Crystal Structure of SARS-CoV-2 main protease in complex with NCL-00023830
5RF0	Crystal Structure of SARS-CoV-2 main protease in complex with POB0073
5REZ	Crystal Structure of SARS-CoV-2 main protease in complex with POB0129
5REY	Crystal Structure of SARS-CoV-2 main protease in complex with PCM-0102911
5REX	Crystal Structure of SARS-CoV-2 main protease in complex with PCM-0102287

5REW	Crystal Structure of SARS-CoV-2 main protease in complex with PCM-0102275
5REV	Crystal Structure of SARS-CoV-2 main protease in complex with PCM-0103072
5REU	Crystal Structure of SARS-CoV-2 main protease in complex with PCM-0102395
5RET	Crystal Structure of SARS-CoV-2 main protease in complex with PCM-0102269
5RES	Crystal Structure of SARS-CoV-2 main protease in complex with PCM-0102281
5RER	Crystal Structure of SARS-CoV-2 main protease in complex with PCM-0102615
5REP	Crystal Structure of SARS-CoV-2 main protease in complex with PCM-0102201
5REO	Crystal Structure of SARS-CoV-2 main protease in complex with PCM-0102578
5REN	Crystal Structure of SARS-CoV-2 main protease in complex with PCM-0102425
5REM	Crystal Structure of SARS-CoV-2 main protease in complex with PCM-0103016
5REL	Crystal Structure of SARS-CoV-2 main protease in complex with PCM-0102340
5REK	Crystal Structure of SARS-CoV-2 main protease in complex with PCM-0102327
5REJ	Crystal Structure of SARS-CoV-2 main protease in complex with PCM-0102241
5REI	Crystal Structure of SARS-CoV-2 main protease in complex with Z2856434856
5REH	Crystal Structure of SARS-CoV-2 main protease in complex with Z111507846
5REG	Crystal Structure of SARS-CoV-2 main protease in complex with Z1545313172
5REF	Crystal Structure of SARS-CoV-2 main protease in complex with Z24758179
5REE	Crystal Structure of SARS-CoV-2 main protease in complex with Z2217052426
5RED	Crystal Structure of SARS-CoV-2 main protease in complex with Z2856434865
5REC	Crystal Structure of SARS-CoV-2 main protease in complex with Z1587220559
5REB	Crystal Structure of SARS-CoV-2 main protease in complex with Z2856434899
5REA	Crystal Structure of SARS-CoV-2 main protease in complex with Z31432226
5RE9	Crystal Structure of SARS-CoV-2 main protease in complex with Z2856434836
5RE8	Crystal Structure of SARS-CoV-2 main protease in complex with Z2737076969
5RE7	Crystal Structure of SARS-CoV-2 main protease in complex with Z30932204
5RE6	Crystal Structure of SARS-CoV-2 main protease in complex with Z54571979
5RE5	Crystal Structure of SARS-CoV-2 main protease in complex with Z33545544
5RFK	Crystal Structure of SARS-CoV-2 main protease in complex with PCM-0102575
5RFL	Crystal Structure of SARS-CoV-2 main protease in complex with PCM-0102389
5RFM	Crystal Structure of SARS-CoV-2 main protease in complex with PCM-0102539
5RFN	Crystal Structure of SARS-CoV-2 main protease in complex with PCM-0102868
5RFO	Crystal Structure of SARS-CoV-2 main protease in complex with PCM-0102972
5RFP	Crystal Structure of SARS-CoV-2 main protease in complex with PCM-0102190
5RFQ	Crystal Structure of SARS-CoV-2 main protease in complex with PCM-0102179
5RFR	Crystal Structure of SARS-CoV-2 main protease in complex with PCM-0102169
5RFS	Crystal Structure of SARS-CoV-2 main protease in complex with PCM-0102739
5RFT	Crystal Structure of SARS-CoV-2 main protease in complex with PCM-0102432
5RFU	Crystal Structure of SARS-CoV-2 main protease in complex with PCM-0102121

5RFV	Crystal Structure of SARS-CoV-2 main protease in complex with PCM-0102306
5RFU	Crystal Structure of SARS-CoV-2 main protease in complex with PCM-0102121
5RFT	Crystal Structure of SARS-CoV-2 main protease in complex with PCM-0102432
5RFS	Crystal Structure of SARS-CoV-2 main protease in complex with PCM-0102739
5RFR	Crystal Structure of SARS-CoV-2 main protease in complex with PCM-0102169
5RFQ	Crystal Structure of SARS-CoV-2 main protease in complex with PCM-0102179
5RFP	Crystal Structure of SARS-CoV-2 main protease in complex with PCM-0102190
5RFO	Crystal Structure of SARS-CoV-2 main protease in complex with PCM-0102972
5RFN	Crystal Structure of SARS-CoV-2 main protease in complex with PCM-0102868
5RFM	Crystal Structure of SARS-CoV-2 main protease in complex with PCM-0102539
5RFL	Crystal Structure of SARS-CoV-2 main protease in complex with PCM-0102389
5RFK	Crystal Structure of SARS-CoV-2 main protease in complex with PCM-0102575
6Y2F	Crystal structure (monoclinic form) of the complex resulting from the reaction between SARS-CoV-2 (2019-nCoV) main protease and tert-butyl (1-((S)-1-(((S)-4-(benzylamino)-3,4-dioxo-1-((S)-2-oxopyrrolidin-3-yl)butan-2-yl)amino)-3-cyclopropyl-1-oxopropan-2-yl)-2-oxo-1,2-dihydropyridin-3-yl)carbamate (alpha-ketoamide 13b)
6Y2G	Crystal structure (orthorhombic form) of the complex resulting from the reaction between SARS-CoV-2 (2019-nCoV) main protease and tert-butyl (1-((S)-1-(((S)-4-(benzylamino)-3,4-dioxo-1-((S)-2-oxopyrrolidin-3-yl)butan-2-yl)amino)-3-cyclopropyl-1-oxopropan-2-yl)-2-oxo-1,2-dihydropyridin-3-yl)carbamate (alpha-ketoamide 13b)
6VSB	Prefusion 2019-nCoV spike glycoprotein with a single receptor-binding domain up
6LVN	Structure of the 2019-nCoV HR2 Domain
6M03	The crystal structure of COVID-19 main protease in apo form
6W63	Structure of COVID-19 main protease bound to potent broad-spectrum non-covalent inhibitor X77
6M71	2019-nCoV RNA-dependent RNA polymerase in complex with cofactors
5R80	Crystal Structure of COVID-19 main protease in complex with Z18197050
6LU7	The crystal structure of COVID-19 main protease in complex with an inhibitor N3
5R7Y	Crystal Structure of COVID-19 main protease in complex with Z45617795
5R7Z	Crystal Structure of COVID-19 main protease in complex with Z1220452176
5R81	Crystal Structure of COVID-19 main protease in complex with Z1367324110
5R82	Crystal Structure of COVID-19 main protease in complex with Z219104216
5R83	Crystal Structure of COVID-19 main protease in complex with Z44592329
5R84	Crystal Structure of COVID-19 main protease in complex with Z31792168
6VW1	Structure of 2019-nCoV chimeric receptor-binding domain complexed with its



	receptor human ACE2
6M0J	Crystal structure of 2019-nCoV spike receptor-binding domain bound with ACE2
6M17	The 2019-nCoV RBD/ACE2-B0AT1 complex
6Y84	SARS-CoV-2 main protease with unliganded active site (2019-nCoV, coronavirus disease 2019, COVID-19)
6YB7	SARS-CoV-2 main protease with unliganded active site (2019-nCoV, coronavirus disease 2019, COVID-19)
6Y2E	Crystal structure of the free enzyme of the SARS-CoV-2 (2019-nCoV) main protease
6W75	1.95 Angstrom Resolution Crystal Structure of NSP10 - NSP16 Complex from SARS-CoV-2
6W61	Crystal Structure of the methyltransferase-stimulatory factor complex of NSP16 and NSP10 from SARS CoV-2.
6W4H	1.80 Angstrom Resolution Crystal Structure of NSP16 - NSP10 Complex from SARS-CoV-2
6M3M	Crystal structure of SARS-CoV-2 nucleocapsid protein N-terminal RNA binding domain
6VYO	Crystal structure of RNA binding domain of nucleocapsid phosphoprotein from SARS coronavirus 2
6W9Q	Peptide-bound SARS-CoV-2 Nsp9 RNA-replicase
7BTF	SARS-CoV-2 RNA-dependent RNA polymerase in complex with cofactors in reduced condition
6YI3	The N-terminal RNA-binding domain of the SARS-CoV-2 nucleocapsid phosphoprotein

The list provides the PDBID with description of crystal structures of proteins in SARS-CoV-2 deposited in PDB (as on April 11, 2020)

**Table 2: Details of proteome of SARS-Cov-2**

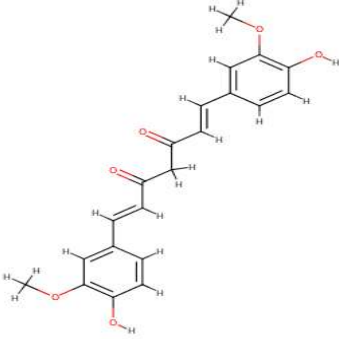
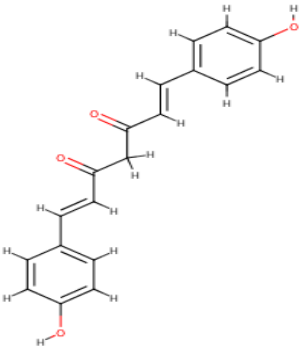
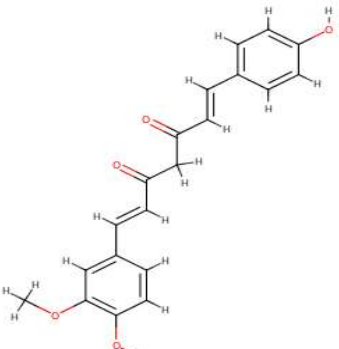
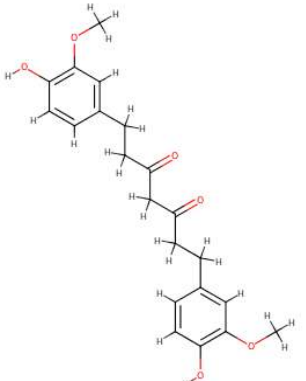
<b>Protein Name</b>	<b>Length</b>	<b>Mature Protein</b>	<b>PDB Structure</b>
<b>orf1ab polyprotein</b>	7096	NSP1 (Leader Protein)	NO
		NSP2	NO
		NSP3 (papain-like proteinase, ADP ribose phosphatase)	YES
		NSP4	NO
		NSP5A and NSP5B (3C-like proteinase)	YES
		NSP6	NO
		NSP7	YES
		NSP8	YES
		NSP9 (ssRNA-binding protein)	YES
		NSP10	IN COMPLEX WITH NSP16
		NSP12 (RNA-dependent RNA polymerase)	YES
		NSP13 (helicase)	NO
		NSP14 (exonuclease)	NO
		NSP15 (endoRNase)	NO
		NSP16 (2'-O-ribose methyltransferase)	IN COMPLEX WITH NSP10
<b>orf1a polyprotein</b>	4405	NSP1 (Leader Protein)	NO
		NSP2	NO
		NSP3 (papain-like proteinase, ADP ribose phosphatase)	YES
		NSP4	NO
		NSP5A and NSP5B (3C-like proteinase)	YES
		NSP6	NO
		NSP7	YES
		NSP8	YES
		NSP9 (ssRNA-binding protein)	YES
		NSP10	IN COMPLEX WITH NSP16
NSP11	NO		
<b>Surface glycoprotein</b>	1273	Surface (spike) glycoprotein	YES
<b>ORF3a protein</b>	275	ORF3a protein	NO
<b>Envelope protein</b>	75	Envelope protein	NO
<b>Membrane glycoprotein</b>	222	Membrane glycoprotein	NO
<b>ORF6 protein</b>	61	ORF6 protein	NO
<b>ORF7a protein</b>	121	ORF7a protein	NO
<b>ORF7b</b>	43	ORF7b	NO
<b>ORF8 protein</b>	121	ORF8 protein	NO

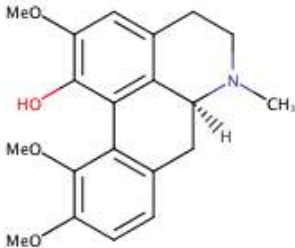
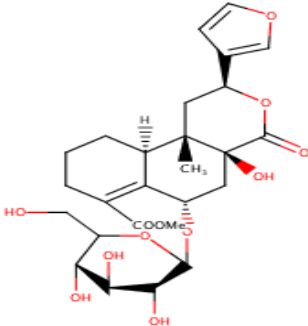
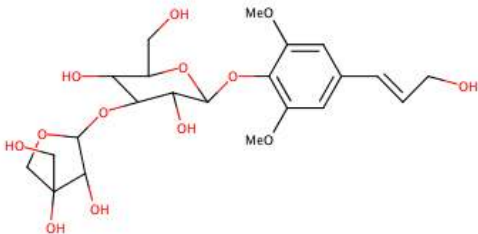
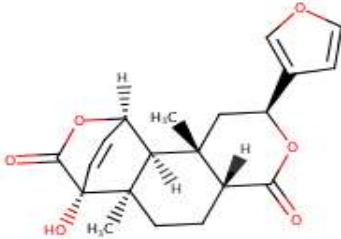
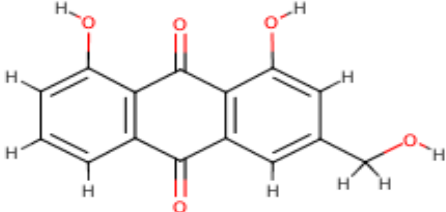
<b>Nucleocapsid phosphoprotein</b>	419	Nucleocapsid phosphoprotein	YES
<b>ORF10 protein</b>	38	ORF10 protein	NO

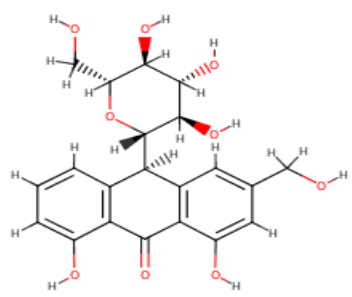
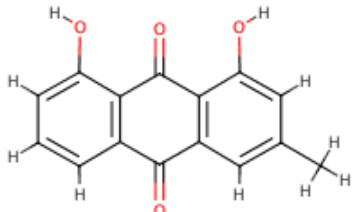
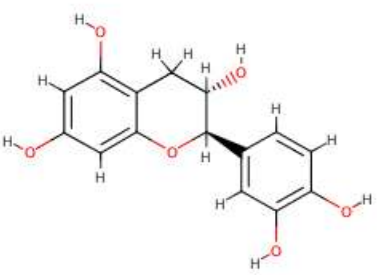
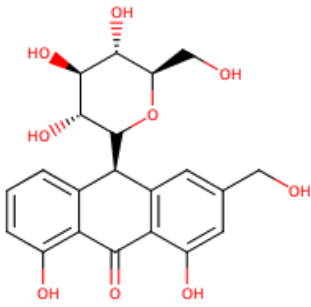
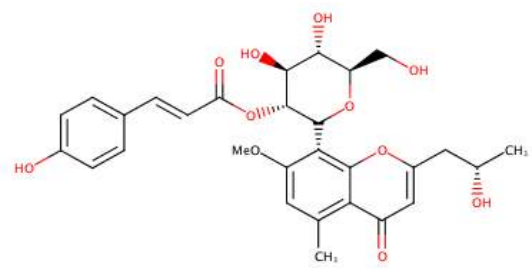
The list provides proteins details of SARS-CoV-2 as obtained from GenBank: NC\_045512.2

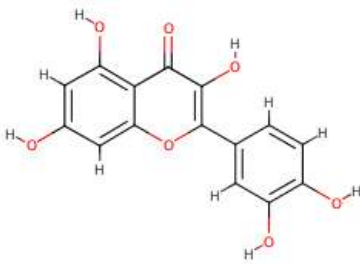
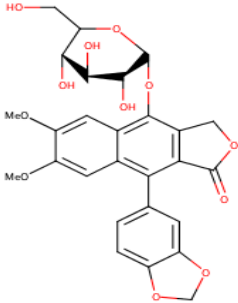
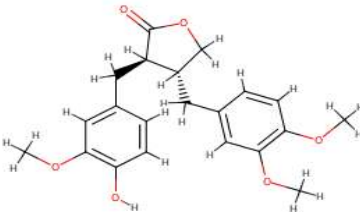
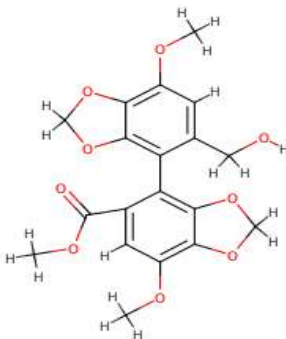
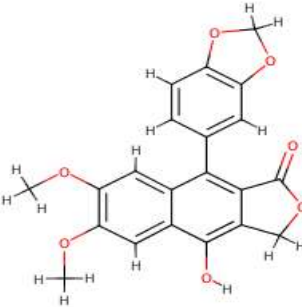
**Table 3: List of ligands used for docking studies**

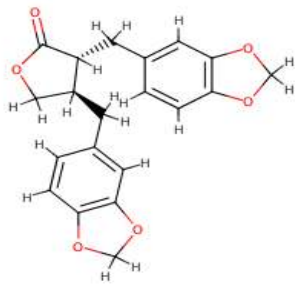
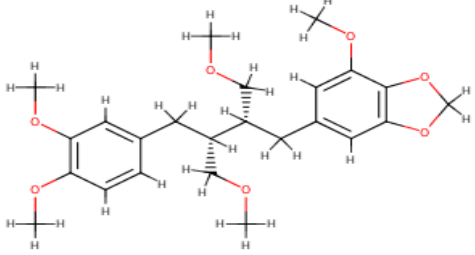
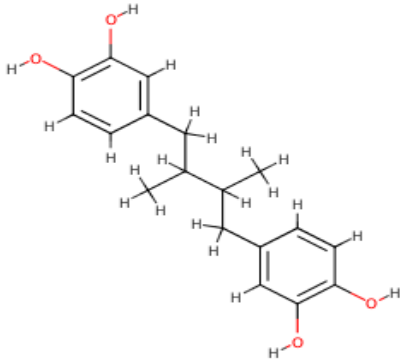
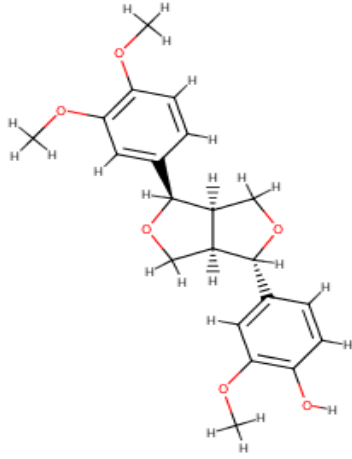
The list provides the names of ligands with 2D structures screened by molecular docking with target proteins in SARS-CoV-2. The ligands 1-30 include phytochemicals compiled from medicinal plants and the ligands 31-37 are the repurposed drugs (with 2D structures) currently in use for treatment of COVID-19 infection.

S.No.	Ligands	2D structure
Phytochemicals in Medicinal Plants		
1.	Curcumin	 <p>The image shows the 2D chemical structure of Curcumin. It consists of two phenyl rings connected by a central heptadiene chain. Each phenyl ring has two hydroxyl groups (-OH) at the 2 and 6 positions. The heptadiene chain is in its open-chain form, with two double bonds and a central carbon-carbon single bond.</p>
2.	Bisdemethoxycurcumin	 <p>The image shows the 2D chemical structure of Bisdemethoxycurcumin. It is similar to curcumin but has only one hydroxyl group (-OH) on each phenyl ring, located at the 2-position.</p>
3.	Demethoxycurcumin	 <p>The image shows the 2D chemical structure of Demethoxycurcumin. It is similar to curcumin but has only one hydroxyl group (-OH) on each phenyl ring, located at the 6-position.</p>
4.	Tetrahydrocurcumin	 <p>The image shows the 2D chemical structure of Tetrahydrocurcumin. It is similar to curcumin but has four hydrogen atoms added to the heptadiene chain, making it a saturated chain. The phenyl rings have hydroxyl groups (-OH) at the 2 and 6 positions.</p>
5.	Corydine	

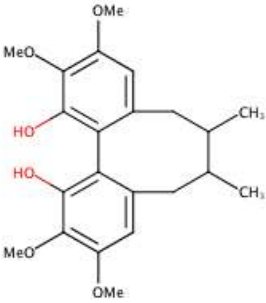
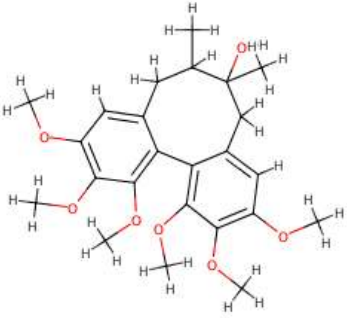
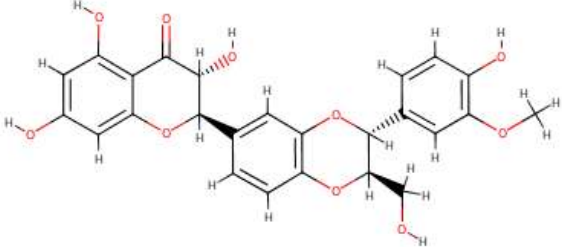
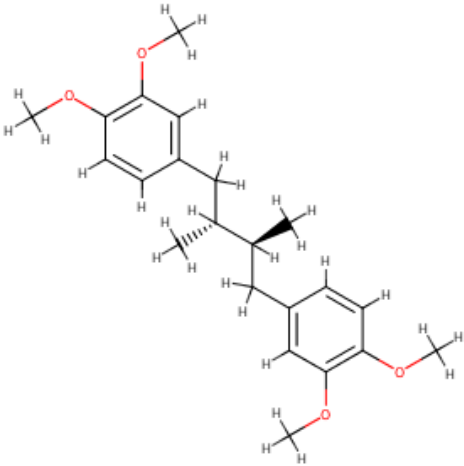
		 <p>The structure shows a complex polycyclic system with a central benzene ring fused to two other rings. It features three methoxy (MeO) groups and one hydroxyl (HO) group on the benzene ring. A piperidine ring is fused to the system, with a methyl group (CH<sub>3</sub>) and a hydrogen atom (H) attached to the nitrogen atom.</p>
6.	Cordioside	 <p>The structure is a complex polycyclic molecule with multiple stereocenters. It features a central ring system with a methyl group (CH<sub>3</sub>) and a hydroxyl group (OH). A side chain contains a furfuryl group and a methyl group. A methyl ester group (COOMe) is also present.</p>
7.	Cordiofolioside A	 <p>The structure shows a complex polycyclic system with a central benzene ring. It features two methoxy (MeO) groups and a hydroxyl group (OH) on the benzene ring. A side chain contains a furfuryl group and a methyl group. A methyl ester group (COOMe) is also present.</p>
8.	Tinosporin	 <p>The structure is a complex polycyclic molecule with multiple stereocenters. It features a central ring system with a methyl group (H<sub>3</sub>C) and a hydroxyl group (OH). A side chain contains a furfuryl group and a methyl group.</p>
9.	Aloe-emodin	 <p>The structure shows a complex polycyclic system with a central benzene ring. It features two hydroxyl groups (OH) and a methyl group (H<sub>3</sub>C) on the benzene ring. A side chain contains a furfuryl group and a methyl group.</p>
10.	Aloin	

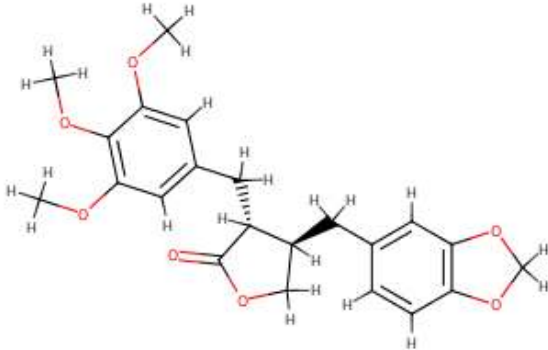
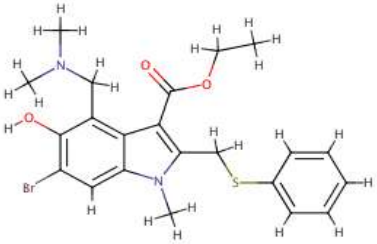
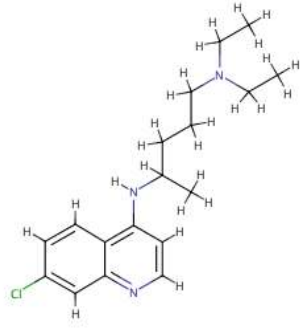
		
11.	Chrysophanol	
12.	Catechin	
13.	Aloin A	
14.	Isoaloesin	
15.	Quercetin	

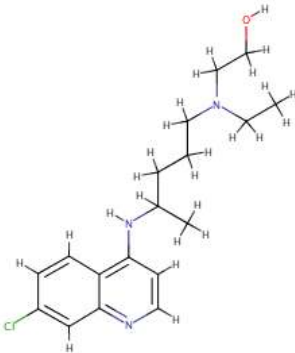
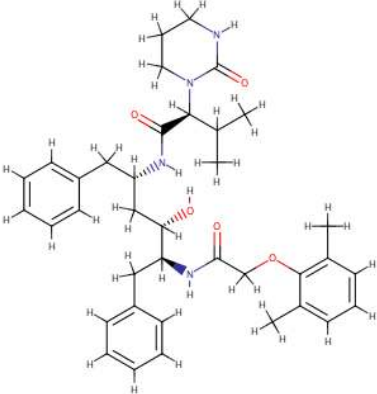
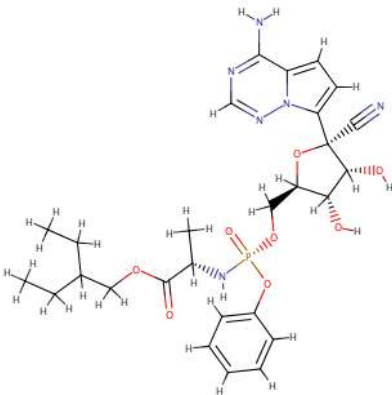

		 <p>The structure shows two pyrogallol units (1,2,3-trihydroxybenzene) linked by an ether bridge at their 4-positions. Each pyrogallol unit has hydroxyl groups at the 1, 2, and 3 positions.</p>
16.	6-deoxyglucose-diphyllin	 <p>The structure features a diphyllin core with a 6-deoxyglucopyranoside moiety attached to one of the pyrogallol units. The glucose ring is shown in its cyclic form with a hydroxyl group at C5 and a hydroxymethyl group at C6. The diphyllin core has methoxy groups at the 4-positions of the pyrogallol units.</p>
17.	Arctigenin	 <p>The structure is a complex polycyclic molecule consisting of two pyrogallol units linked by an ether bridge. It features a central five-membered ring system and several hydroxyl groups, including one at the 4-position of one of the pyrogallol units.</p>
18.	Bicyclol	 <p>The structure consists of two pyrogallol units linked by an ether bridge. Each pyrogallol unit has hydroxyl groups at the 1, 2, and 3 positions, and the ether bridge connects the 4-positions of both units.</p>
19.	Diphyllin	 <p>The structure shows two pyrogallol units linked by an ether bridge at their 4-positions. Each pyrogallol unit has hydroxyl groups at the 1, 2, and 3 positions.</p>
20.	Hinokinin	

		
21.	Niranthin	
22.	Nordihydroguaiaretic acid	
23.	Phillygenin	
24.	Rubrifloralignin A	



		 <p>The structure shows two benzene rings connected by a seven-membered ring. Each benzene ring has a methoxy group (MeO) at the 1 and 3 positions and a hydroxyl group (HO) at the 2 position. The seven-membered ring has two methyl groups (CH<sub>3</sub>) at the 4 and 5 positions.</p>
25.	Schisandrin	 <p>The structure shows a complex polycyclic system with multiple fused rings and several hydroxyl groups (HO) attached to the rings.</p>
26.	Silybin	 <p>The structure shows a complex polycyclic system with multiple fused rings and several hydroxyl groups (HO) attached to the rings.</p>
27.	Terameprocol	 <p>The structure shows a complex polycyclic system with multiple fused rings and several hydroxyl groups (HO) attached to the rings.</p>
28.	Yatein	

		
29.	Withaferin A	
30.	Withanolide A	
Repurposed Drugs		
31.	Arbidol	
32.	Chloroquine	
33.	Hydroxychloroquine	

		 <p>The image shows the chemical structure of Lopinavir, a protease inhibitor. It features a central chromane ring system with a chlorine atom at the 7-position. Attached to the chromane are two piperidine rings, one of which is further substituted with a hydroxymethyl group.</p>
34.	Lopinavir	 <p>The image shows the chemical structure of Remdesivir, a nucleoside analog. It consists of a ribose sugar ring with a cytosine base at the C1 position, a phosphonate group at the C3 position, and a 2'-deoxyadenosine moiety at the C5 position.</p>
35.	Remdesivir	 <p>The image shows the chemical structure of Ribavirin, a nucleoside analog. It features a ribose sugar ring with a cytosine base at the C1 position, a phosphonate group at the C3 position, and a 2'-deoxyadenosine moiety at the C5 position.</p>
36.	Ribavirin	 <p>The image shows the chemical structure of Ritonavir, a protease inhibitor. It features a central chromane ring system with a chlorine atom at the 7-position. Attached to the chromane are two piperidine rings, one of which is further substituted with a hydroxymethyl group.</p>
37.	Ritonavir	

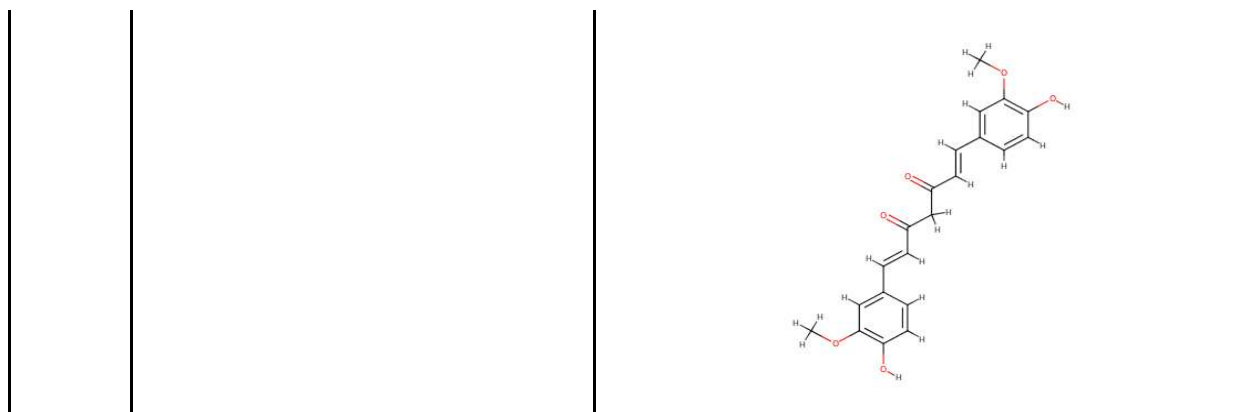


**Table 4: Amino acid residues in the binding site of Spike protein and RNA polymerase**

The table lists the amino acid residues identified in the binding pocket of Spike protein and predicted by CASTp server for RNA polymerase

Target protein	Binding site residues
Interface residues of spike receptor binding domain with ACE2	LYS 417, VAL 445, GLY 446, GLY 447, TYR 449, TYR 453, LEU 455, PHE 456, TYR 473, ALA 475, GLY 476, GLU 484, PHE 486, ASN 487, TYR 489, GLN 493, GLY 496, GLN 498, THR 500, ASN 501, GLY 502, TYR 505
RNA-dependent RNA-polymerase	ASP 164, VAL 166, GLU 167, LYS 438, HIS 439, PHE 441, ASP 452, TYR 455, TYR 456, ILE 494, ASN 496, ASN 497, ASP 499, LYS 500, SER 501, GLY 503, ASN 507, LYS 511, THR 540, GLN 541, MET 542, ASN 543, LEU 544, LYS 545, TYR 546, ALA 547, ILE 548, SER 549, ALA 550, LYS 551, ARG 553, ALA 554, ARG 555, THR 556, VAL 557, ALA 558, GLY 559, THR 565, ASN 568, ARG 569, HIS 572, GLN 573, LEU 576, LYS 577, ALA 580, VAL 588, ILE 589, GLY 590, THR 591, SER 592, LYS 593, PHE 594, TRP 598, MET 601, LEU 602, GLY 616, TRP 617, ASP 618, TYR 619, PRO 620, LYS 621, CYS 622, ASP 623, ARG 624, GLU 665, VAL 667, LYS 676, THR 680, SER 681, SER 682, GLY 683, ASP 684, ALA 685, THR 686, THR 687, ALA 688, TYR 689, ASN 691, MET 756, LEU 758, SER 759, ASP 760, ASP 761, ALA 762, VAL 763, VAL 792, PHE 793, SER 795, ALA 797, LYS 798, CYS 799, TRP 800, HIS 810, GLU 811, PHE 812, CYS 813, SER 814, GLN 815, HIS 816, ASP 833, SER 835, ARG 836, ILE 837, ALA 840, GLY 841, PHE 843, VAL 844, ASP 845, LEU 854, MET 855, GLU 857, ARG 858, PHE 859, SER 861, LEU 862, ILE 864, ASP 865

**Table 5: Molecular docking of ligands (phytochemicals and repurposed drugs) with target proteins of SARS-CoV-2 using FLARE.** The table shows the binding energy values (in kcal/mol) of ligands (phytochemicals) docked to all three target proteins, namely main protease, Spike glycoprotein and RNA polymerase in SARS-CoV-2. The repurposed drugs were docked to their respective drug targets as shown. The

highlighted values in the table denote the higher binding energy values of phytochemical-docked complexes in comparison to repurposed drug –target complexes.

Ligands		Protease (PDB ID: 6W63)	Spike glycoprotein - ACE2 (PDB ID: 6M0J)	RNA-dependent RNA- polymerase (PDB ID: 6M71)
<b>Curcumin and its derivatives</b>	Curcumin	-8.104	-6.278	<b>-7.556</b>
	Bisdemethoxy-curcumin	-8.424	-8.436	<b>-7.698</b>
	Demethoxycurcumin	-8.611	-8.642	<b>-7.565</b>
	Tetrahydrocurcumin	-8.793	-8.009	<b>-7.518</b>
<b>Constituents of <i>Tinospora cordifolia</i></b>	Corydine	-7.91	-6.041	-6.942
	<b>Cordioside</b>	<b>-10.577</b>	-8.77	-8.142
	Cordiofolioside A	-8.02	-6.964	-7.657
	Tinosporin	-7.924	-7.288	-7.553
<b>Constituents of Aloe Vera</b>	Aloe-emodin	-7.784	-5.888	-7.283
	Aloin	-9.185	-8.383	-8.889
	Chrysophanol	-7.322	-6.153	-6.895
	<b>Catechin</b>	-9.582	<b>-9.243</b>	-7.264
	Aloin A	-9.533	-8.432	-8.761
	Isoaloesin	-9.759	-7.835	-8.492
	<b>Quercetin</b>	-7.78	-8.664	<b>-9.131</b>
<b>Constituents of Silymarin</b>	<b>Silybin</b>	<b>-11.928</b>	<b>-10.572</b>	<b>-11.499</b>
<b>Ashwagandha (<i>Withania somnifera</i>)</b>	<b>Withaferin A</b>	<b>-11.242</b>	<b>-9.631</b>	<b>-9.27</b>
	<b>Withanolide A</b>	<b>-10.292</b>	-8.708	<b>-9.668</b>
<b>Lignans</b>	6-deoxyglucose-diphyllin	-8.495	-7.241	-7.487
	Arctigenin	-8.456	-8.055	-7.766
	Bicyclol	-7.906	-7.042	-7.464
	Diphyllin	-8.508	-7.917	-7.339
	Hinokinin	-7.665	-7.106	-7.025
	Niranthin	-9.333	-8.463	-7.287
	Nordihydroguaiaretic acid	-9.018	-7.696	-8.39
	<b>Phillygenin</b>	-9.503	<b>-9.102</b>	-7.807
	Rubrifloralignin A	-9.236	-7.868	-8.221
	Schisandrin	-9.056	-7.189	-8.386
	Terameprocol	-7.778	-7.203	-7.363
	Yatein	-8.236	-7.373	-6.939
<b>Repurposed Drugs currently used in treating COVID-19</b>	Arbidol	NA	-8.913	NA
	Chloroquine	NA	-8.019	NA
	Hydroxychloroquine	NA	-7.862	NA
	Lopinavir	-9.71	NA	NA
	Remdesivir	NA	NA	-6.02
	Ribavirin	NA	NA	-5.229
	Ritonavir	-9.135	NA	NA

# Figures

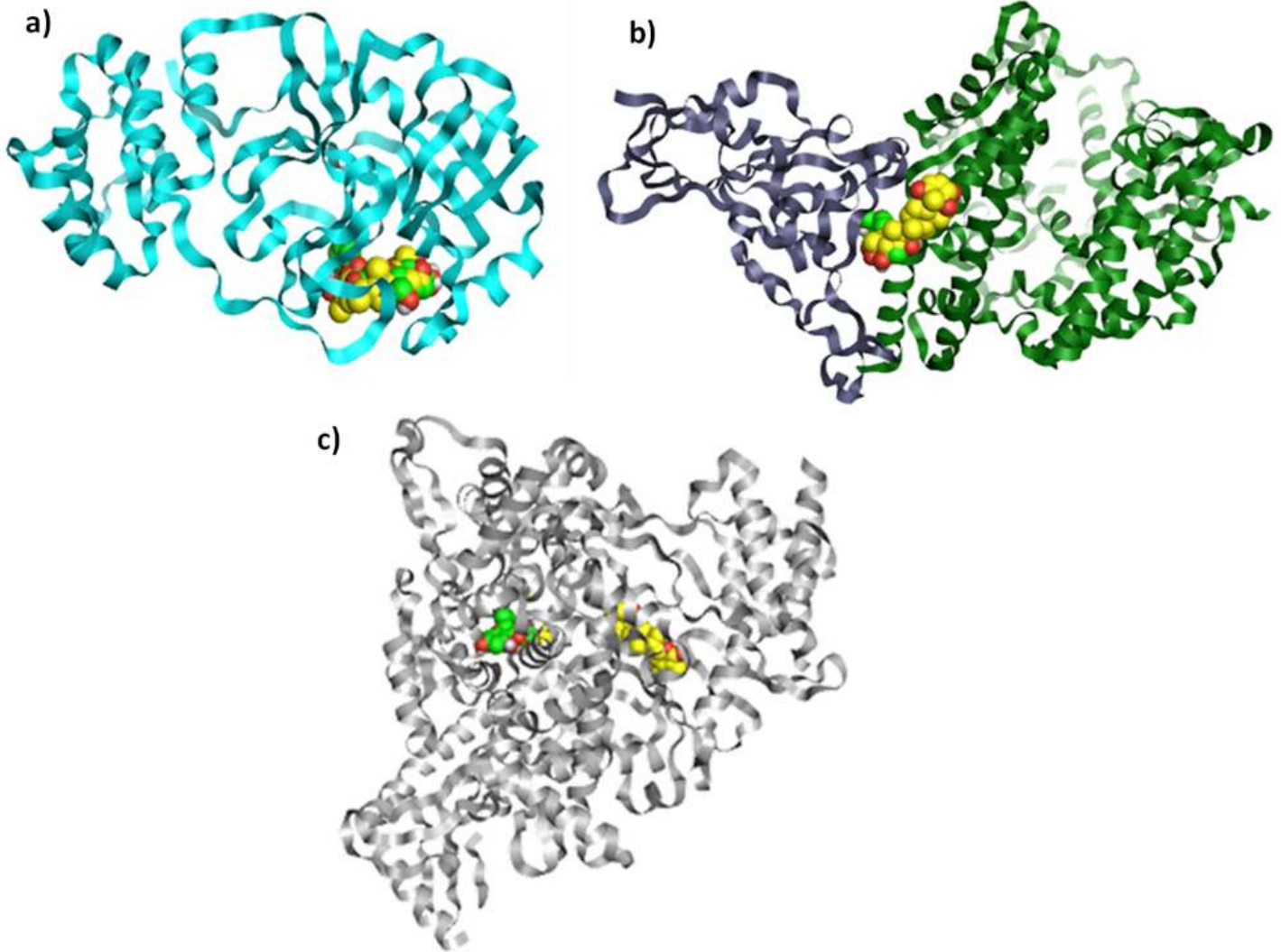


**Figure 1**

The figure shows Silybin (green) and Withaferin A (yellow CPK model) docked to a) main protease (PDB ID: 6W63), b) Spike glycoprotein-ACE2 (PDB ID: 6M0J) and c) RNA-dependent RNA-polymerase (PDB ID: 6M71)

